CHEMISTRY
A EUROPEAN JOURNAL

FULL PAPER

DOI: 10.1002/chem.201204062

On the Mechanism of the Dehydroaromatization of Hexane to Benzene by an Iridium Pincer Catalyst

Akanksha Thawani,[a] Ramanan Rajeev,[b] and Raghavan B. Sunoj*[b]

Abstract: The developments in the area of transition-metal pincer complexes have opened up new avenues for conversion of saturated hydrocarbons to more useful aromatic compounds under homogeneous reaction conditions. In the backdrop of an interesting series of conversions of unbranched alkanes to benzene, toluene, and xylene (known as the BTX family aromatics) reported by Goldman and co-workers (*Nature Chem.* **2011**, *3*, 167), we herein present a comprehensive mechanistic picture obtained by using density functional computations. The reaction involves an iridium–PCP-pincer-catalyzed dehydroaromatization of hexane to benzene (in which PCP = η^3-C_6H_3(*i*PrP)$_2$-1,3) by using *tert*-butylethylene (TBE) as a sacrificial acceptor. The most energetically preferred pathway for a sequence of dehydrogenations is identified to begin with a terminal C–H bond activation of *n*-hexane leading to the formation of hex-1-ene. Although the initial dehydrogenation of *n*-hexane was found to be endergonic, the accompanying exoergic hydrogenation of TBE to *tert*-butylethane (TBA) compensates the energetics to keep the catalytic cycle efficient. Subsequent dehydrogenations provide a hexa-1,3-diene and then a hexa-1,3,5-triene. The pincer bound triene is identified to undergo cyclization to furnish cyclohexadiene. Eventually, dehydrogenation of cyclohexa-1,3-diene offers benzene. In the most preferred pathway, the Gibbs free energy barrier for cyclization leading to the formation of cyclohexa-1,3-diene is found to exhibit the highest barrier (21.7 kcal mol^{-1}).

Keywords: C–H activation · dehydroaromatization · density functional calculations · reaction mechanisms · transition states

Introduction

Over the years, several attempts have been made in converting saturated hydrocarbons, a richly abundant constituent in petroleum feedstock, to more valuable cyclic aromatic compounds by using heterogeneous catalysis. Most of these approaches involving catalytic dehydrogenation and aromatization employed high temperatures (≈500 °C).[1] In the recent past, a class of tridentate compounds known as pincers have received increasing attention as potential ligands for homogeneous catalysts for alkane dehydrogenation.[2] In particular, the bis-phosphine η^3-C_6H_3(*i*PrP)$_2$-1,3 (PCP) class of pincers have emerged as robust ligands capable of offering thermally stable catalysts with transition metals such as iridium. Iridium pincers have been in use for alkane dehydrogenation for more than a decade.[3a–f] In one of the earliest reports, Kaska and Jensen[3g] employed Ir-pincers in conjunction with *tert*-butylethene (TBE) as an acceptor for alkane dehydrogenation. The mechanistic[4] and computational studies on these reactions have suggested the involvement of an associative as well as dissociative pathways.[5] There have been efforts toward the development of acceptorless dehydrogenation reactions as well.[4e] An interesting aspect of metal-catalyzed dehydrogenation methods is that it can provide access to terminal alkenes, which are otherwise difficult to generate by using standard reactions. The problem is particularly acute for aryl systems because Friedel Craft's alkylations would lead to branched alkyl chains, owing to the higher stability of secondary carbocations that are involved in the mechanism of such reactions.

In a very recent report, Goldman and Brookhart[6] have demonstrated that arenes could be produced from higher alkanes by using an iridium–PCP pincer catalyst and *tert*-butylethylene as an acceptor. The invention is quite promising and could be regarded as capable of providing future technological impetus in this direction. Improved understanding of the mechanism of this reaction might help enable commercial exploitation leading to production of benzene, toluene, xylene (known as the BTX family), and higher arenes from petroleum feedstock. The chemistry therefore assumes additional significance in an era of depleting fossil fuels.

The mechanism of formation and the associated energetics for the conversion of linear alkanes to arenes has not been established yet. Herein, results of our density functional study on PCP–Ir–H_4 catalyzed conversion of *n*-hexane to benzene with the help of TBE as the sacrificial acceptor, are

[a] A. Thawani
Department of Chemical Engineering
Indian Institute of Technology Bombay
Powai, Mumbai 400076 (India)

[b] Dr. R. Rajeev, Prof. Dr. R. B. Sunoj
Department of Chemistry
Indian Institute of Technology Bombay
Powai, Mumbai 400076 (India)
E-mail: sunoj@chem.iitb.ac.in

Supporting information for this article is available on the WWW under http://dx.doi.org/10.1002/chem.201204062.

reported. It was established earlier that during the conversion of hexane to benzene, *tert*-butylethylene (TBE) undergoes hydrogenation to *tert*-butylethane (TBA).[3e–g] Four moles of TBE is consumed for every mole of conversion of *n*-hexane to benzene.[7] The energetically more-favored dissociative pathway is emphasized in the present study.[8] The overall reaction can be viewed as the conversion of *n*-hexane to benzene, through a series of consecutive catalytic dehydrogenations to hexa-1,3,5-triene followed by an electrocyclization and dehydrogenation to yield benzene, as shown in Scheme 1. One molecule of active catalyst PCP–Ir

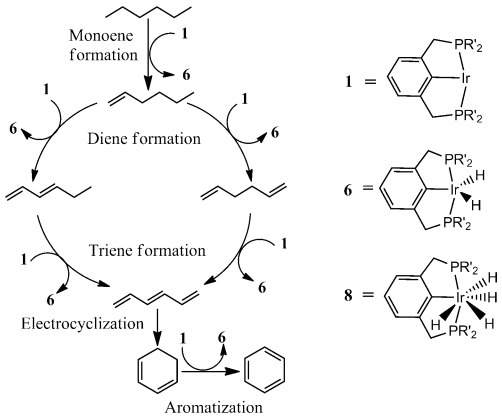

Scheme 1. Catalytic dehydrogenation of *n*-hexane to hexa-1,3,5-triene and subsequent dehydroaromatization to benzene.

(**1**) is converted into PCP–Ir–H_2 (**6**) for each dehydrogenation event. The dihydro-iridium intermediate **6**, in turn, can consume a molecule of H_2 liberated in the initial conversion of **8** to **6**, and facilitate the regeneration of the pre-catalyst PCP–Ir–H_4 (**8**). More information on important elementary steps and the accompanying details of the key stationary points are depicted in Scheme 2.

Results and Discussion

The mechanism can be considered as beginning with the interaction of *n*-hexane with the coordinatively unsaturated active catalyst PCP–Ir (**1**). Although the pincer can exist as different conformers, the most stable conformer is chosen for the mechanistic investigations reported in this study.[9] The substrate *n*-hexane can bind to **1** either through its terminal methyl or internal methylene groups. The weakly bound pre-reacting complex leading to the terminal C–H activation is designated as **2**. An α-agostic interaction between iridium and terminal methyl group is identified in **2**. The C–H bond length of the interacting methyl group is found to be longer (1.12 Å) as compared with the non-interacting C–H bonds (1.09 Å). The barrier for the terminal C–H bond activation, computed as the difference in energy between **2** and **TS(2–3)**, is 13.2 kcal mol^{-1}. The transition-state geometry for the C–H activation as well as some of the key intermediates are provided in Figure 1. Intermediate **3**, gen-

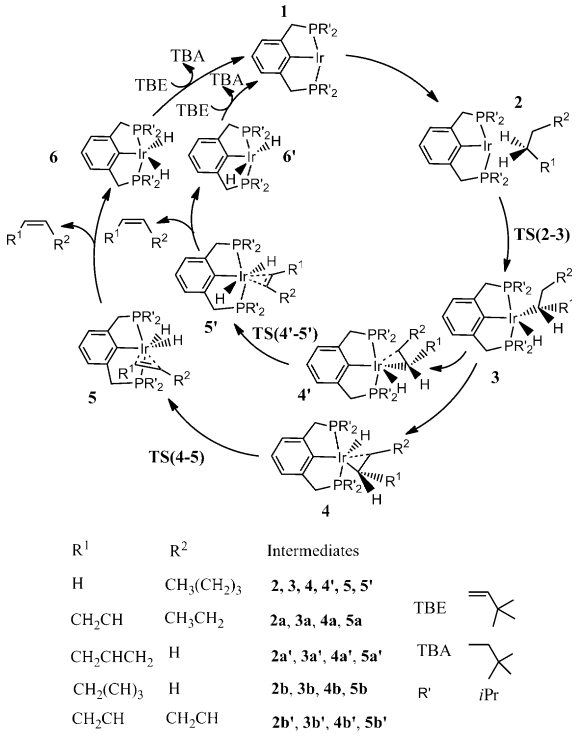

Scheme 2. A plausible mechanism for the conversion of an alkane to an alkene by PCP–Ir.

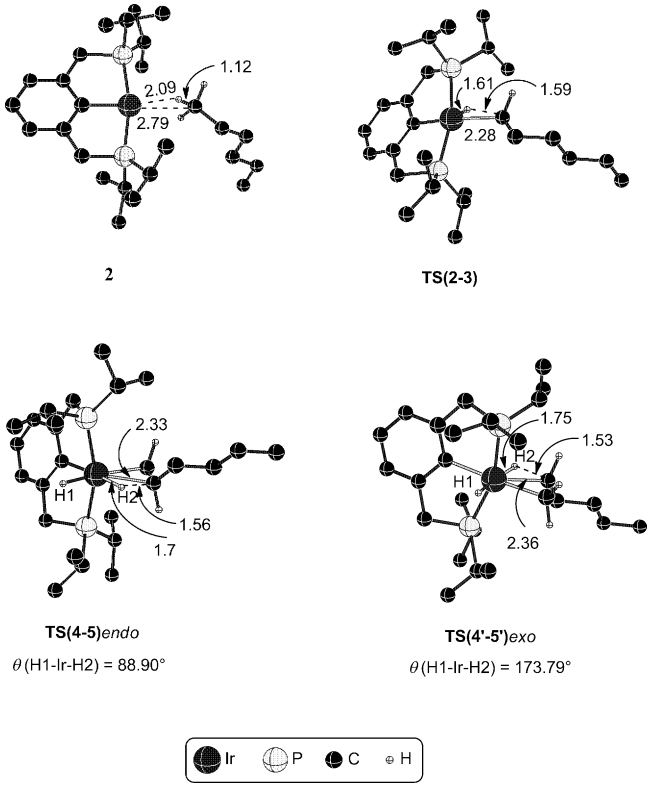

Figure 1. The geometries of intermediate **2** and the transition states for the key steps involved in the catalytic cycle. Selected bond lengths (Å) and angles (°) are given. Only selected hydrogen atoms are shown for improved clarity.

erated via this step, consists of a hexyl chain and a hydrogen bound to the iridium center.

Other conformers of the iridium-alkyl intermediate **3** exhibiting a β-agostic interaction, denoted as **4** and **4′**, are also identified. The agostic interaction is identified to be stronger in **4** (activated C–H bond length) than in **4′**. In intermediate **4**, β-(C–H), (β-H)–Ir, and Ir–(β-C) bond distances are 1.14, 2.23, and 2.64 Å, respectively, whereas in **4′**, longer Ir–C (3.14 Å), Ir–H (3.19 Å) and shorter C–H (1.10 Å) bond distances are noticed. The vital olefination step can now occur in intermediate **4** (or **4′**) through a β-H transfer involving **TS(4–5)** (or **TS(4′–5′)**). Depending on the relative positions and the angle between the hydrogen atoms and the alkyl chain on iridium (θ), two key geometric possibilities, *endo* and *exo*, are considered. The *endo* and *exo* geometries denote an acute and obtuse H–Ir–H angle, respectively (Figure 1). It can be readily noticed from the Gibbs free energy profile, as given in Figure 2, that the barrier for the

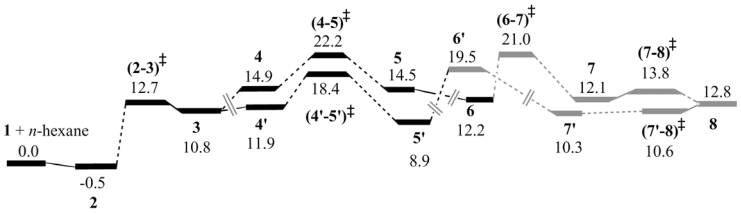

Figure 2. The Gibbs free energy profile (in kcal mol^{-1}) for the formation of **5** (or **5′**) from *n*-hexane catalyzed by **1**, and regeneration of the pre-catalyst **8** (in grey).[12]

conversion of **4′** to **5′** in the *exo* pathway is found to be 6.6 kcal mol^{-1}, whereas that for **4** to **5** in the *endo* pathway is 7.3 kcal mol^{-1}.[10] The products **5′** and **5** are η^2-complexes of hex-1-ene with PCP–Ir–H_2 in *exo* and *endo* geometries, respectively. The relative energies of π-olefin complexes **5** and **5′** indicate that the *exo* product complex **5′** is more stable than the corresponding *endo* complex **5**.[11] At this stage, the product of the first catalytic cycle, namely hex-1-ene, should be released such that the regeneration of the catalyst is facilitated.

The expulsion of hex-1-ene from **5** (or **5′**) would give rise to an endoergic PCP–Ir–H_2 species **6** (or **6′**). The intermediates **6** and **6′** differ mainly in the H–Ir–H angle, which were found to be 59 and 176°, respectively.[13] The likely conversion of **6** (or **6′**) to pre-catalyst **8** as well as the active catalyst **1** is summarized in Scheme 3. It is important to note at this juncture that H_2 liberated during the course of generation of the active species PCP–Ir (**1**), facilitated by TBE to TBA conversion, can develop a weak interaction with **6** (or **6′**). The reactive PCP–Ir–H_2 could therefore form a σ-complex with a molecular hydrogen to give way to an intermediate PCP–Ir–H_4 (**7**). The Gibbs free energy barrier as given by **TS(6–7)** for the hydrogen uptake in the *endo* pathway is 8.8 kcal mol^{-1} (Figure 2). The optimized geometry of **TS(6–7)** is provided in Figure 3a. The analogous transition-state in the *exo* pathway could not be optimized even after repeated

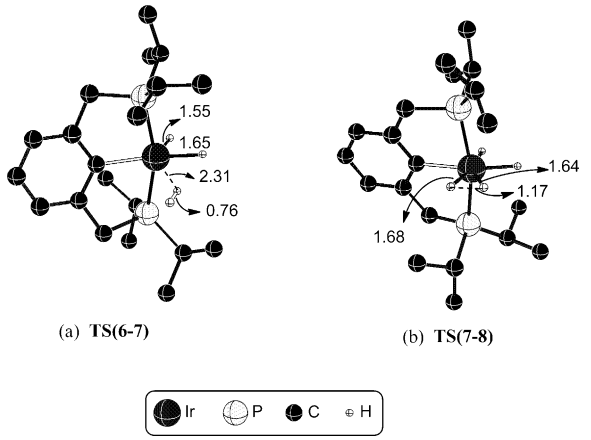

Figure 3. Transition-state geometries for the formation of a) the σ-complex with molecular hydrogen and b) the subsequent conversion to PCP–Ir–H_4. All distances are in Å.

attempts. These σ-complexes (**7** and **7′**) can collapse to the original pre-catalyst PCP–Ir–H_4 (**8**) through a relatively low barrier process. The geometry of the corresponding transition state, **TS(7–8)**, is provided in Figure 3b. One catalytic cycle can be considered as complete with the regeneration of the pre-catalyst **8** through the aforementioned steps.

The discussions thus far have been on the formation of hex-1-ene from hexane. However, an alternative possibility leading to an internal olefin, such as hex-3-ene cannot be ruled out. Computed energetics predict that the activation

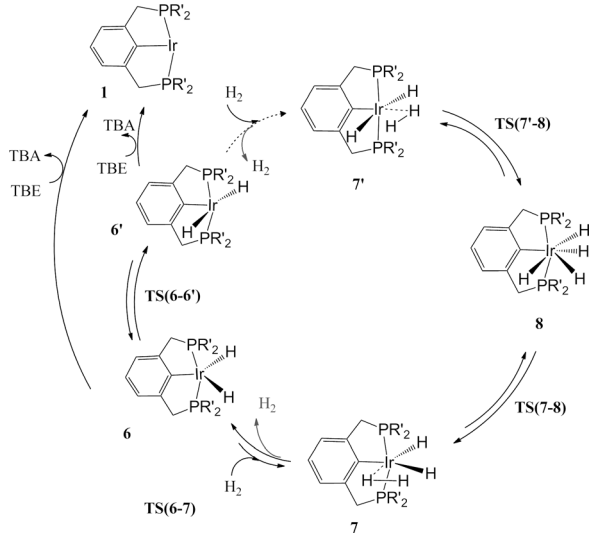

Scheme 3. A plausible mechanism for catalyst regeneration from PCP–Ir–H_2 (**6** or **6′**) formed as a result of the first step of olefination of *n*-hexane to hex-1-ene.

of C–H bonds at C2 or C3 positions are less favorable as compared to that noticed for the terminal position.[14] The relative energies of the transition states for the C–H activations at C1, C2, and C3 positions are found to be 12.7, 16.7, and 19.9 kcal mol^{-1}, respectively.

A similar series of mechanistic steps, as in the formation of hex-1-ene, is envisaged toward producing higher analogues such as dienes and triene. Depending on the relative positions of further C–H activations, the formation of hexa-1,3,5-triene can follow two key sequences. The second dehydrogenation of hex-1-ene can lead either to hexa-1,3-diene or hexa-1,5-diene. Each of these dienes upon subsequent dehydrogenation would furnish the desired hexa-1,3,5-triene. Beginning from hex-1-ene, either C3–H or C4–H activation followed by a dehydrogenation can give hexa-1,3-diene. The allylic C3–H activation is found to be more favored over the homoallylic C4–H activation. The improved stabilization of the incipient partial charges in the transition state for allylic C–H bond activation, as revealed by NPA analysis, can be regarded as the key reason for such a preference.[15] Hexa-1,5-diene can be formed only through terminal C6–H activation of hex-1-ene because of steric issues described earlier.

In view of these possibilities, the following mechanistic sequence is examined for the conversion of hexene to hexadiene. Since the type of mechanistic steps involved is similar to the first dehydrogenation leading to olefin, the nomenclature adopted here employs "**a**" preceded by the corresponding numerical identifier for different species (Scheme 2). These include 1) the formation of a weakly interacting complex (**2a**) between the catalytically active species **1** and hex-1-ene, 2) oxidative insertion leading to an iridium-alkyl species (**3a**), 3) conformational change to **4a**, 4) β-H transfer to furnish the diene bound to PCP–Ir–H_2 (**5a**), and 5) separation of the respective diene from **5a** giving way to **6a**. In the β-H transfer step, the formation of *endo* and *exo* isomers is possible.

The Gibbs free energy profile for dehydrogenation of hex-1-ene to the corresponding dienes is provided in Figure 4. The lower energy transition-states, **TS(4a–5a)** and **TS(4a′–5a′)**, belonging only to the *endo* and *exo* pathways, respectively, are included in the profile. The relative energy of the higher energy **TS(4a–5a)** in the corresponding *exo* pathway for the formation of hexa-1,3-diene is found to be

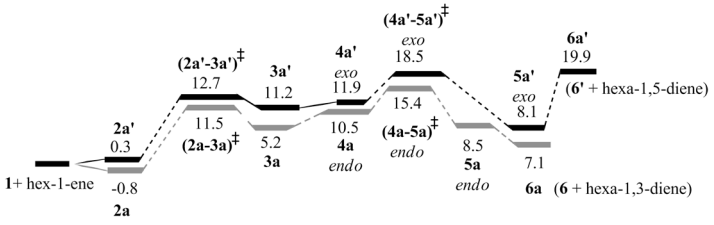

Figure 4. Gibbs free energy profile (in kcal mol^{-1}) for the formation of hexa-1,3-diene (**2a**–**6a**; in grey) and hexa-1,5-diene (**2a′**–**6a′**; in black) from hex-1-ene. The energies are with respect to **1** and hex-1-ene.[16] Conversion of **6′** to **6** follows the sequence as shown earlier in Scheme 3.

18.1 kcal mol^{-1}. Similarly higher energy transition-state for the formation of hexa-1,5-diene, **TS(4a′–5a′)**, in the *endo* route is as high as 22.0 kcal mol^{-1}.

It can be noticed form the Gibbs free energy profile that there are no exoergic intermediates (except **2a** with just less than kcal mol^{-1} of stabilization) involved in the overall dehydrogenation process. The highest energy transition-state **TS(4a–5a)***endo* in energetically the most preferred pathway can therefore be regarded as the rate-limiting transition-state for hexa-1,2-diene to hexa-1,3-diene conversion.[17] Examination of the elementary step barriers for the C–H activation in both hexa-1,3-diene (**TS(2a–3a)**) and hexa-1,5-diene (**TS(2a′–3a′)**) pathways conveys no particular kinetic advantage in favor of 1,3- or 1,5-diene. However, the relative free energies of the transition states for the next β-H transfer step in hexa-1,5-diene pathway is 18.5 kcal mol^{-1} as compared with 15.4 kcal mol^{-1} in hexa-1,3-diene pathway, suggesting that the formation of hexa-1,3-diene is more likely. The optimized geometries of these transition states, **TS(4a′–5a′)***exo* and **TS(4a–5a)***endo*, are provided in Figure 5. Comparison of the geometries, particularly around the reaction coordinate at which the hydrogen transfer occurs, reveals nearly identical structural features. Hence, the relative energy difference of 3.1 kcal mol^{-1} between two the transition states should be regarded as arising due to improved conjugation of the developing double bond in the case of **TS(4a–5a)**. Another pathway for isomerization of hex-1-ene to hex-2-ene is also examined.[18] It is important to note that the free energy of dehydrogenation of hexane, which is the energy gap between two catalytic cycles, (15.2 kcal mol^{-1}) can be regarded as compensated by the hydrogenation of TBE (24.1 kcal mol^{-1}).

Now that hexadiene is produced, one more cycle of dehydrogenation would provide hexa-1,3,5-triene. To this end, both C5–H and C6–H activations in hexa-1,3-diene are examined first. The Gibbs free energy profile for the conversion of hexa-1,3-diene to hexa-1,3,5-triene is provided in Figure 6. The free energy of **TS(2b″–3b″)** for C5–H activation and the subsequent oxidative insertion step to C6–H bond via **TS(4b″–5b″)** are lower than that of **TS(2b–3b)** and **TS(4b–5b)**. The preference is more pronounced in the energy difference between **TS(4b″–5b″)** and **TS(4b–5b)**, suggesting that the reaction sequence involving the C5–H oxidative insertion first, followed by C6–H oxidative insertion, is more likely to operate.[19] It is found that the electronic effects dominate over steric effect and the energetics for the initial step favors allylic C5–H activation. The optimized geometries of **TS(2b″–3b″)** and **TS(4b″–5b″)***exo* are provided in Figure 7. The product complexes **5b** and **5b″** obtained through **TS(4b–5b)** and **TS(4b″–5b″)**, respectively, are the two different conformers of the pincer-alkene complex.[20] The other stationary points such as **3b″** and **4b″** refer to the two key conformers of the iridium-alkyl intermediate, whereas **5b″** is a π-complex between hexa-1,3,5-triene and PCP–Ir bound through a C3–C4 double bond. It is important to note that after each olefination, the product (hex-1-ene, hexa-1,3-diene, and hexa-1,3,5-triene) should be

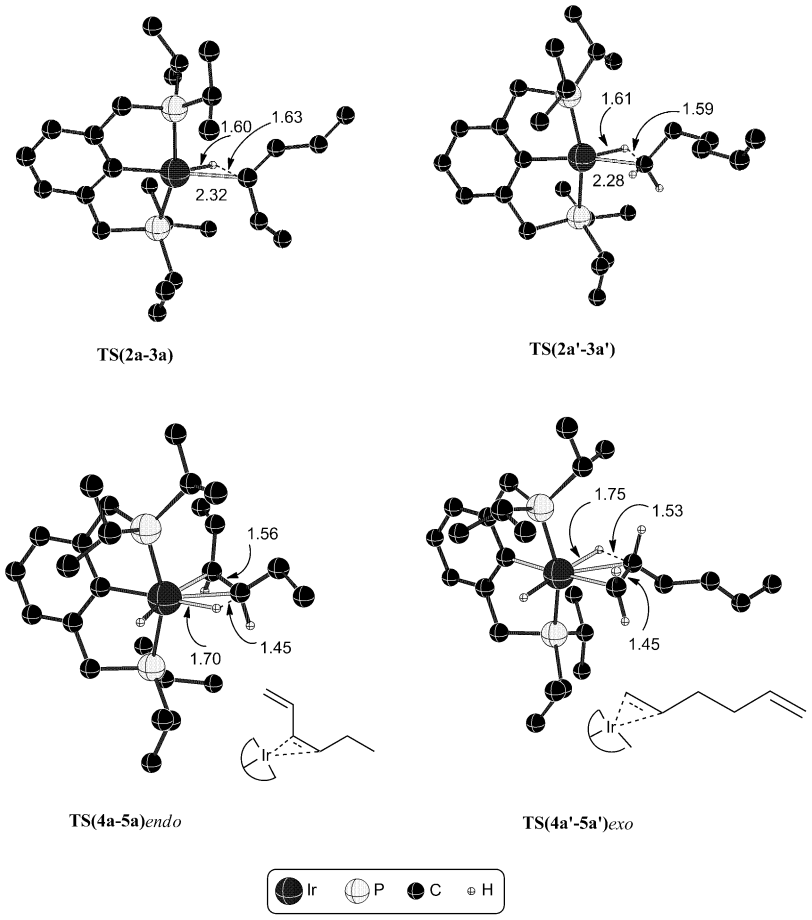

Figure 5. The optimized geometries of the transition states involved in hexa-1,3-diene and hexa-1,5-diene formation. All distances are given in Å.

released from the corresponding PCP–Ir–H_2 complex to sustain the catalytic cycle through the regeneration steps by **6** to **1** conversion facilitated by the hydrogenation of TBE (Scheme 2).

The penultimate step to aromatization involves an electrocyclization of hexa-1,3,5-triene. The ensuing cyclohexa-1,3-diene upon dehydrogenation would provide benzene as the final product. The Gibbs free energy of the transition state for electrocyclization reveals a barrier of 22.6 kcal mol^{-1}. Electrocyclization could as well take place in a pincer bound hexa-1,3,5-triene. An intermediate **5c** is located, which is a weakly bound complex of hexa-1,3,5-triene with **1** through an activated C–H bond. The electrocyclization of **5c** furnishes a η^2-complex of cyclohexa-1,3-diene with **1** (**5d**). The barrier for **5c**–**5d** conversion is found to be 21.7 kcal mol^{-1} (Figure 8).[21] Thus, the conversion of hexatriene to cyclohexadiene, though the **5c** to **5d** pathway is slightly preferred over a direct electrocyclization.

Lastly, in the aromatization step, cyclohexa-1,3-diene first develops an α-agostic interaction with the iridium center as shown in **2e** (Figure 8). The stationary points **3e** and **4e** represent two conformers of iridium-cyclohexyl intermediates in the *endo* pathway formed through the oxidative insertion of the active catalyst **1** to one of the methylene groups of cyclohexa-1,3-diene. Compound **4e** gives way to a complex between benzene and (PCP)Ir–H_2 (**5e**), through a low barrier process. Increased steric interaction between the isopropyl of the pincer and cyclohexyl (in the transition state) or benzene (in the product complex) is noticed. The energetic advantage of this step arises due to the formation of stable and aromatic benzene as the product.[22] Interestingly, the energy of the separated **6e** and benzene is

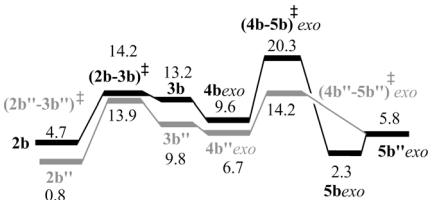

Figure 6. Gibbs free energy profile (in kcal mol^{-1}) for the conversion of hexa-1,3-diene to hexa-1,3,5-triene. The grey curve represents C5–H activation whereas the black one represents C6–H activation. Compound **2b″** is the pre-reacting complex for C5–H activation. **4b″** is another conformer of **3b″** in the *exo* pathway.

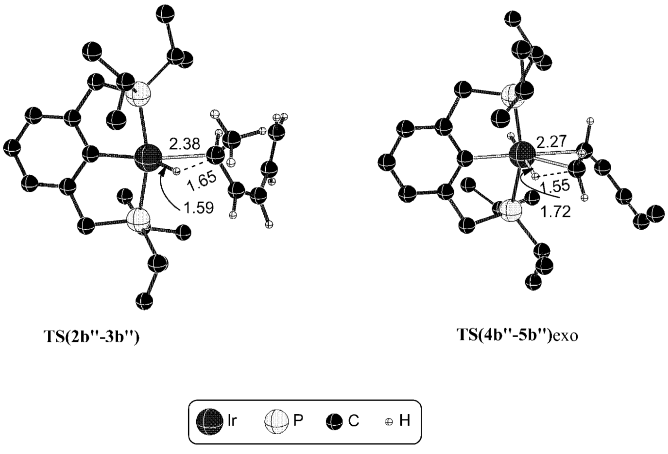

Figure 7. The optimized geometries of the transition states for the formation of hexa-1,3,5-triene from hexa-1,3-diene. All distances are given in Å.

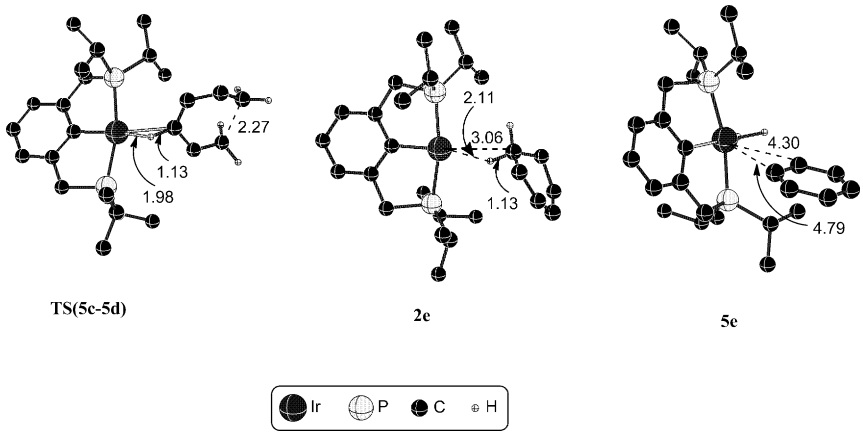

Figure 8. Transition-state geometries and intermediates involved in the cyclization and aromatization of hexa-1,3,5-triene and cyclohexa-1,3-diene, respectively. All distances are given in Å.

found to be more stable by 25.0 kcal mol^{-1} as compared with the original reference point (**1** and cyclohexa-1,3-diene), indicating that the overall reaction is thermodynamically feasible (Figure 9). Geometries of the transition states involved in the step are given in Figure 10.

The likely participation of η3-allylic intermediates in aromatization/dearomatization pathways: In light of a few recent reports that aromatization and de-aromatization of pincer backbone could as well take place under certain reaction conditions, we have explored the likely involvement of such pathways for the dehydrogenation.[23] It is of significance to note that de-aromatization of PNP-pincers are suggested to be involved in the catalytic cycle for the oxidation of water or in the reduction of CO_2. However, such possibilities with PCP-pincers are expected to be higher in energy. Changes in the normal valence of carbon or nitrogen coordinating to the metal can bring vital differences.[24] A complete catalytic cycle, including participation by de-aromatized pincer, for the conversion of *n*-hexane to hexa-1,3,5-triene is provided in Scheme 4.

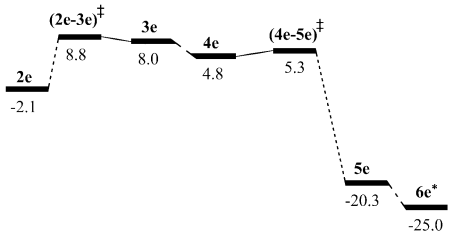

Figure 9. Gibbs free energy (in kcal mol^{-1}) profile for aromatization of cyclohexa-1,3-diene to benzene. **6e*** is **6** inclusive of benzene.

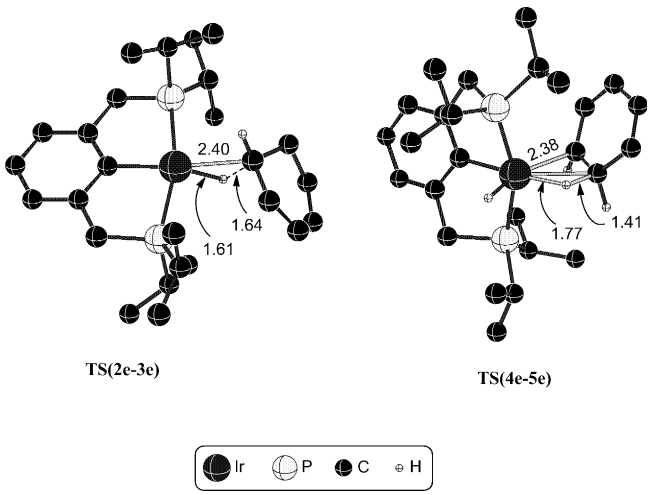

Figure 10. Transition-state geometries involved in the aromatization of cyclohexa-1,3-diene to benzene. All distances are given in Å.

The iridium-alkyl intermediate **3** obtained from the previous steps (see above) can undergo insertion to an internal γ-methylene (C3–H) to give intermediate **20** with two hydrogen atoms bound to the iridium. Subsequent reductive elimination results in the expulsion of a molecular hydrogen to furnish an iridacycle intermediate **21**. The activation of internal C2–H bond in **21** can now furnish a η^3-coordinated π-allyl type intermediate **22**. A combination of the hydrogen atoms bound to iridium and that from the methylene of the PCP ligand in **22** can help release a molecule of H_2. Consideration of this dehydrogenation possibility through **TS(22–13)** can now provide a de-aromatized pincer **13**.

Alternatively, intermediate **13** can be generated through a different route, starting from intermediate **3**. In this pathway, de-aromatization occurs first in intermediate **3** that provides an iridium-alkyl intermediate **9**. Oxidative insertion to C2–H leads to a metal-olefin intermediate **10**. Subsequent hydrogen migration involving **TS(10–11)** will help regain the aromaticity in **11**. Oxidative insertion to the C3–H bond converts **11** to a η^3-coordinated π-allyl type intermediate **12**. Dehydrogenation involving pincer methylene hydrogen and the hydrogen bound to iridium converts **12** to **13** through **TS(12–13)**. The resulting de-aromatized π-allyl intermediate **13** can then undergo C4–H insertion to provide **14**, which is a diene bound to iridium. A similar sequence of reactions, such as C–H insertion, de-aromatization and expulsion of molecular hydrogen, and hydrogen migration, and aromatization can follow for the conversion of hexa-1,3-diene to hexa-1,3,5-triene (**19**). Displacement of product hexatriene by a new molecule of *n*-hexane will help continue the catalytic cycle.

The Gibbs free energy profile summarizing the energetics of formation of hexatriene involving de-aromatization of the pincer ligand is provided in Figure 11. The most noticeable feature of this pathway is that all the transition states are of

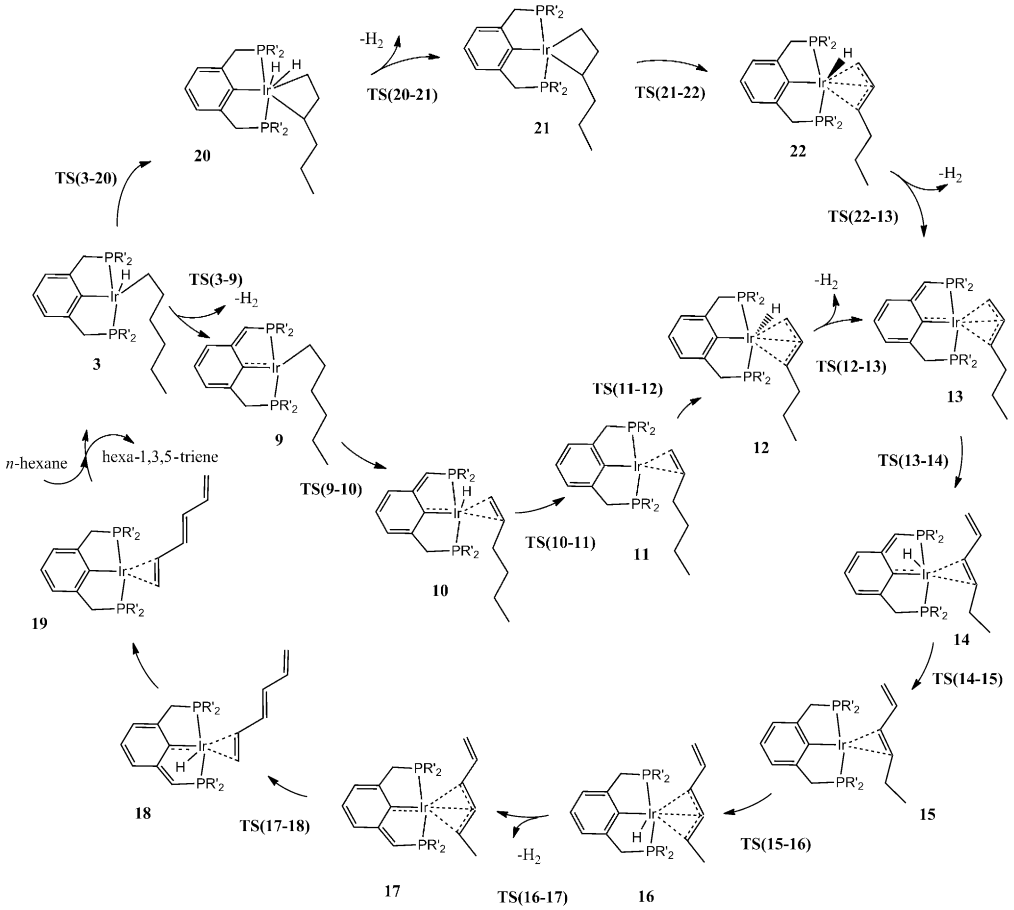

Scheme 4. A plausible mechanism for the conversion of *n*-hexane to hexa-1,3,5-triene involving aromatization/dearomatization of the Ir–PCP pincer.

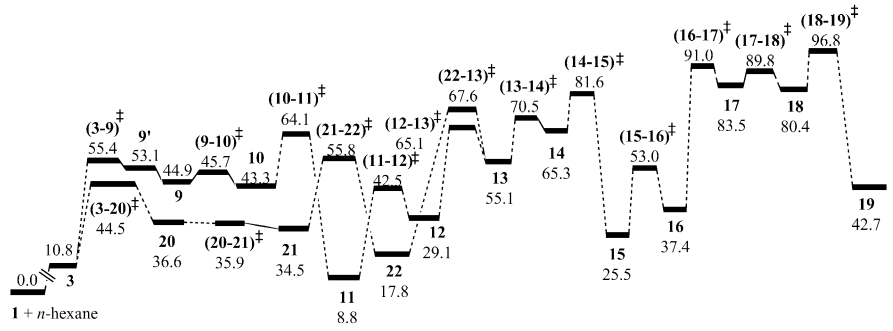

Figure 11. Gibbs free energy profile (in kcal mol^{-1}) for the conversion of *n*-hexane to hexa-1,3,5-triene involving aromatization/dearomatization of the Ir–PCP pincer.

much higher energy as compared to the sequence of dehydrogenations presented in the preceding section. The Gibbs free energies of the de-aromatized intermediates (such as **9**, **10**, **13**, **14**, **17**, and **18**) are in the range of 40 to 80 kcal mol^{-1}. It is therefore highly suggestive that the reaction cannot proceed through de-aromatization, unlike in the analogous PNP-pincers.[23]

TBE-assisted dehydrogenation: The previous pathways considered the role of TBE in the catalytic cycle as mainly involved in the dehydrogenation of pincer hydride **6**, which is generated in the first place by the dehydrogenation of alkane (Scheme 3). Beginning with the iridium-hexyl intermediate **3**, we now present a possible direct-dehydrogenation pathway enabled by an iridium-bound TBE. Such a direct hydrogen-transfer from *n*-hexane to TBE can occur through two key modes, either involving transition state **TS23** or **TS24**, as shown in Figure 12. In the former transition state, a metal-hydride bond still exists when the hydrogen transfer occurs, whereas in the latter case TBE first forms a σ-bond by transferring the metal-bound hydride and then abstracts the hydrogen from *n*-hexane. The relative Gibbs free energies of both these transition states are found to be more than 52 kcal mol^{-1}. The major contribution to the higher energy of species involved in the TBE-bound pathway arises due to the steric crowding at the iridium center created by the coordination of both hexane and TBE. On the basis of

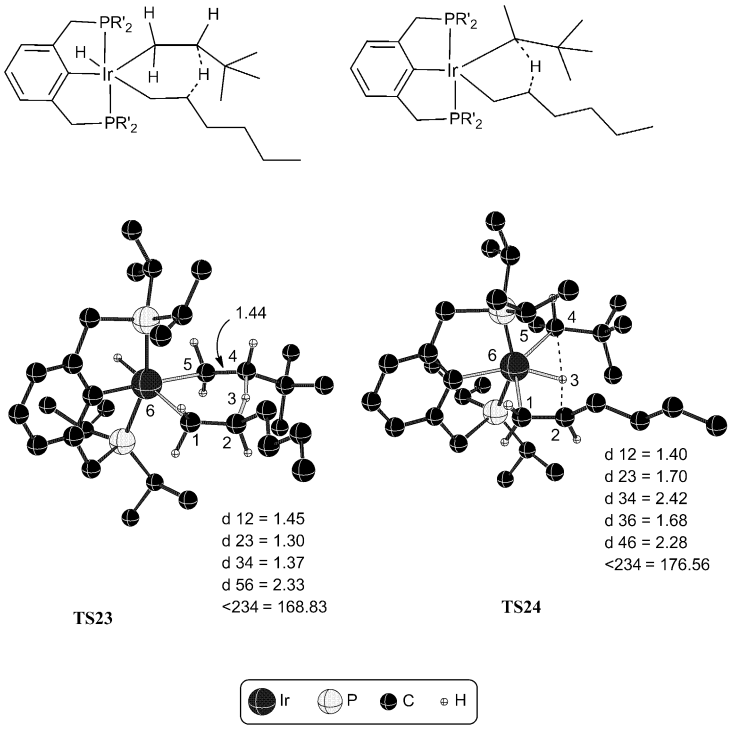

Figure 12. Geometries of the transition states for TBE-assisted dehydrogenation. All distances are given in Å.

the computed higher energy-demand, a direct hydrogen-transfer to TBE should be regarded as an unlikely pathway to operate in the dehydroaromatization of hexane to benzene.

Conclusion

We have identified that the formation of benzene from hexane involved six important steps; the generation of active catalyst **1** through TBE hydrogenation, sequential formation of hexene, hexadiene, and hexatriene, electrocyclization of the resultant triene to cyclohexadiene followed by dehydroaromatization to benzene. The preferred pathway has been identified to involve the formation of hex-1-ene through C1–H bond activation of hexane, hexa-1,3-diene, and hexa-1,3,5-triene. The product of electrocyclization of hexa-1,3,5-triene to cyclohexa-1,3-diene followed by dehydroaromatization by **1** furnishes the desired benzene product. The formation of the η^3-coordinated allylic intermediates and the de-aromatization of the pincer ligand are identified to proceed through higher energy barriers indicating that such mechanisms are less likely to occur with the catalyst and substrate examined in this study. A direct dehydrogenation pathway with a TBE bound to the iridium center is also found to be very high in energy indicating that increasing steric crowding around the metal is not favorable for dehydroaromatization reaction. The overall analysis of the reaction profiles conveys that the electrocyclization of hexa-1,3,5-triene to cyclohexa-1,3-diene presents the highest barrier, implying that the rate of reaction would exhibit a pivotal dependence on the electrocyclization step.

Computational Methods

The geometry optimizations for reactants, intermediates, and transition states was performed in the gas phase with density functional theory (DFT), Becke three-parameter hybrid exchange functional and the Lee–Yang–Parr correlation functional (B3LYP),[25] which is widely used for the calculation of the reaction barrier. The Gaussian 09 suite of quantum chemical programs[26] was used for calculations. The basis set used for carbon, hydrogen, and phosphorus is 6-31G** and Los Alamos pseudopotential basis set (LANL2DZ) for iridium.[27] Whereas 60 inner electrons were treated with an effective core potential (ECP), the remaining 17 valence electrons were explicitly included by using a double zeta quality basis set.[28] Further refinements to the energies, inclusive of improved treatment of dispersive interactions, were performed through single-point energy calculations at the M06/6-311+G**,SDD(Ir) level of theory.[29,30] The Gibbs free energies were obtained by including the thermal and entropic contributions to the single-point energies obtained from the optimized values. All energy values employed for discussions in the text are Gibbs free energies obtained through this approach. All transition states were characterized by one and only one imaginary frequency representing the correct reaction coordinate. The intrinsic reaction coordinate (IRC) calculations were also performed to further authenticate the transition states.[31]

Acknowledgements

Unlimited computing time from the IIT Bombay computer center is gratefully acknowledged.

[1] a) A. Smiešková, E. Rojasová, P. Hudec, L. Šabo, *Appl. Catal. A* **2004**, *268*, 235; b) B. H. Davis, *Catal. Today* **1999**, *53*, 443; c) K. Arata, M. Hino, H. Matsuhashi, *Appl. Catal. A* **1993**, *100*, 19; d) M. Hino, K. Arata, *J. Chem. Soc. Chem. Commun.* **1987**, 1355.

[2] a) S. Biswas, Z. Huang, Y. Choliy, D. Y. Wang, M. Brookhart, K. Krogh-Jespersen, A. S. Goldman, *J. Am. Chem. Soc.* **2012**, *134*, 13276; b) J. Choi, A. H. R. MacArthur, M. Brookhart, A. S. Goldman, *Chem. Rev.* **2011**, *111*, 1761; c) N. Selander, K. J. Szabo, *Chem. Rev.* **2011**, *111*, 2048; d) E. Balaraman, C. Gunanathan, J. Zhang, L. J. W. Shimon, D. Milstein, *Nat. Chem.* **2011**, *3*, 609; f) Z. Huang, P. S. White, M. Brookhart, *Nature* **2010**, *465*, 598; e) H. Nishiyama, J. Ito, *Chem. Commun.* **2010**, *46*, 203; g) M. Käß, A. Friedrich, M. Drees, S. Schneider, *Angew. Chem.* **2009**, *121*, 922; *Angew. Chem. Int. Ed.* **2009**, *48*, 905; h) M. van der Boom, D. Milstein, *Chem. Rev.* **2003**, *103*, 1759.

[3] a) M. W. Haenel, S. Oevers, K. Angermund, W. C. Kaska, F. Hua-Jun, M. B. Hall, *Angew. Chem.* **2001**, *113*, 3708; *Angew. Chem. Int. Ed.* **2001**, *40*, 3596; b) F. Liu, A. S. Goldman, *Chem. Commun.* **1999**, 655; c) M. Gupta, C. Hagen, W. C. Kaska, R. E. Cramer, C. M. Jensen, *J. Am. Chem. Soc.* **1997**, *119*, 840; d) W. Xu, G. P. Rosini, M. Gupta, C. M. Jensen, W. C. Kaska, K. Krogh-Jespersen, A. S. Goldman, *Chem. Commun.* **1997**, 2273; e) I. Göttker-Schnetmann, P. S. White, M. Brookhart, *Organometallics* **2004**, *23*, 1766; f) F. Liu, E. B. Pak, B. Singh, C. M. Jensen, A. S. Goldman, *J. Am. Chem. Soc.* **1999**, *121*, 4086; g) M. Gupta, C. Hagen, R. J. Flesher, W. C. Kaska, C. M. Jensen, *Chem. Commun.* **1996**, 2083; h) R. Rajeev, R. B. Sunoj, *Dalton Trans.* **2012**, *41*, 8430.

[4] a) H. Li, G. Lu, J. Jiang, F. Huang, Z. Wang, *Organometallics* **2011**, *30*, 2349; b) I. Göttker-Schnetmann, M. Brookhart, *J. Am. Chem. Soc.* **2004**, *126*, 9330; c) K. Zhu, P. D. Achord, X. Zhang, K. Krogh-Jespersen, A. S. Goldman, *J. Am. Chem. Soc.* **2004**, *126*, 13044;

d) K. B. Renkema, Y. V. Kissin, A. S. Goldman, *J. Am. Chem. Soc.* **2003**, *125*, 7770; e) K. Krogh-Jespersen, M. Czerw, N. Summa, K. B. Renkema, P. D. Achord, A. S. Goldman, *J. Am. Chem. Soc.* **2002**, *124*, 11404.

[5] a) H.-J. Fan, M. B. Hall, *J. Mol. Catal. A* **2002**, *189*, 111; b) S. Li, M. B. Hall, *Organometallics* **2001**, *20*, 2153; c) S. Niu, M. B. Hall, *J. Am. Chem. Soc.* **1999**, *121*, 3992.

[6] R. Ahuja, B. Punji, M. Findlater, C. Supplee, W. Schinski, M. Brookhart, A. S. Goldman, *Nat. Chem.* **2011**, *3*, 167.

[7] The mechanism of conversion of TBE to TBA is the reverse of the conversion of hexane to hexene, baring the change of the substrate alkane.

[8] It has been reported that the dissociative mechanism is more favorable than the associative pathway at elevated temperatures (see ref. [4e]).

[9] Another key conformer (higher by 3.2 kcal mol^{-1} at the B3LYP/LANL2DZ(Ir),6–31G** level of theory) that differs in the orientation of the phosphorous bound isopropyl groups of the pincer backbone has also been identified.

[10] The energetics for the formation of hex-1-ene are presented in Table S4 in the Supporting Information.

[11] The optimized geometries of **5** (Figure S7) and **5′** (Figure S15) are provided in the Supporting Information. It is noticed that a relatively higher steric interaction between the isopropyl, as well as methylene groups adjacent to P atoms, with the olefinic moiety in **5** results in a slightly distorted geometry, whereas such interactions are minimal in **5′**.

[12] The energies of **6** and **6′** are inclusive of one molecule of hex-1-ene. The energies from **6** (or **6′**) through **8** include the energy of one molecule of hex-1-ene and exclude that of one H_2 molecule.

[13] The barrier for conversion of the lower energy **6** to higher energy **6′** is 22.2 kcal mol^{-1}.

[14] The detailed energetic comparison for the activation of C1–H, C2–H and C3–H bonds is provided in Table S3 in the Supporting Information.

[15] More details on natural charges are provided in Tables S1 and S2 in the Supporting Information.

[16] The energetics for the formation of hexa-1,3-diene and hexa-1,5-diene is provided in Table S5 in the Supporting Information.

[17] Similar interpretations on multi-step reactions can also be found in a) J. R. Murdoch, *J. Chem. Educ.* **1981**, *58*, 32; b) S. Kozuch, S. Shaik, *Acc. Chem. Res.* **2011**, *44*, 101; c) M. Anand, R. B. Sunoj, *Organometallics* **2012**, *31*, 6466.

[18] A two-step isomerization, first from hex-1-ene to hex-2-ene, and then to hex-3-ene is also examined. See Scheme S1, Table S9, and Figure S58 in the Supporting Information.

[19] The energetic details of C5–H activation (Table S6), optimized geometries of stationary points (Figures S32 to S43), and additional transition states involved in triene formation are provided in the Supporting Information. The Gibbs free energy profile for the formation of triene from hexa-1,5-diene is given in Figure S56 in the Supporting Information.

[20] The geometries of **5b** and **5b″** are given in Figure S37 and S43, respectively, in the Supporting Information.

[21] The energies and geometries of **5c**, **5d**, and **TS(5c–5d)** are provided in Table S7 and Figures S44–46, respectively, in the Supporting Information.

[22] The complete energy details of *exo* (**4′e** to **6′e** represents the *exo* pathway) and the *endo* pathways are presented in Table S8 and Figure S57 in Supporting Information. Compound **4′e** is another conformer of **3e** with β-agostic interaction, whereas **5′e** is a complex between benzene and PCP–Ir–H_2, both in the *exo* pathway. Compound **5′e** subsequently gives way to PCP–Ir–H_2 and benzene (**6′e**).

[23] a) J. Li, Y. Shiota, K. Yoshizawa, *J. Am. Chem. Soc.* **2009**, *131*, 13584; b) X. Yang, M. B. Hall, *J. Am. Chem. Soc.* **2010**, *132*, 120; c) R. Tanaka, M. Yamashita, L. W. Chung, K. Morokuma, K. Nozaki, *Organometallics* **2011**, *30*, 6742.

[24] A schematic representation of the changes in the valence state of the nitrogen and carbon atom is given in Scheme S2 in the Supporting Information.

[25] a) A. D. Becke, *Phys. Rev. A* **1988**, *38*, 3098; b) C. Lee, W. Yang, R. G. Parr, *Phys. Rev. B* **1988**, *37*, 785; c) J. P. Perdew, S. H. Chevary, K. A. Vosko, K. A. Jackson, M. R. Pederson, D. J. Singh, C. Fiolhais, *Phys. Rev. B* **1992**, *46*, 6671; d) J. P. Perdew, S. H. Chevary, K. A. Vosko, K. A. Jackson, M. R. Pederson, D. J. Singh, C. Fiolhais, *Phys. Rev. B* **1993**, *48*, 4978; e) A. D. Becke, *J. Chem. Phys.* **1993**, *98*, 5648; f) J. P. Perdew, K. Burke, Y. Wang, *Phys. Rev. B* **1996**, *54*, 16533; g) C. Adamo, V. Barone, *J. Chem. Phys.* **1998**, *108*, 664.

[26] Gaussian 09, Revision A.2, M. J. Frisch, G. W. Trucks, H. B. Schlegel, G. E. Scuseria, M. A. Robb, J. R. Cheeseman, G. Scalmani, V. Barone, B. Mennucci, G. A. Petersson, H. Nakatsuji, M. Caricato, X. Li, H. P. Hratchian, A. F. Izmaylov, J. Bloino, G. Zheng, J. L. Sonnenberg, M. Hada, M. Ehara, K. Toyota, R. Fukuda, J. Hasegawa, M. Ishida, T. Nakajima, Y. Honda, O. Kitao, H. Nakai, T. Vreven, J. A. Montgomery, Jr., J. E. Peralta, F. Ogliaro, M. Bearpark, J. J. Heyd, E. Brothers, K. N. Kudin, V. N. Staroverov, R. Kobayashi, J. Normand, K. Raghavachari, A. Rendell, J. C. Burant, S. S. Iyengar, J. Tomasi, M. Cossi, N. Rega, J. M. Millam, M. Klene, J. E. Knox, J. B. Cross, V. Bakken, C. Adamo, J. Jaramillo, R. Gomperts, R. E. Stratmann, O. Yazyev, A. J. Austin, R. Cammi, C. Pomelli, J. W. Ochterski, R. L. Martin, K. Morokuma, V. G. Zakrzewski, G. A. Voth, P. Salvador, J. J. Dannenberg, S. Dapprich, A. D. Daniels, Ö. Farkas, J. B. Foresman, J. V. Ortiz, J. Cioslowski, D. J. Fox, Gaussian, Inc., Wallingford CT, **2009**.

[27] A. V. Marenich, C. J. Cramer, D. G. Truhlar, *J. Phys. Chem. B* **2009**, *113*, 6378.

[28] a) P. J. Hay, W. R. Wadt, *J. Chem. Phys.* **1985**, *82*, 299; b) P. J. Hay, W. R. Wadt, *J. Chem. Phys.* **1985**, *82*, 270; c) W. R. Wadt, P. J. Hay, *J. Chem. Phys.* **1985**, *82*, 284; d) C. C. Lovallo, M. Klobukowski, *J. Comput. Chem.* **2003**, *24*, 1009; e) L. E. Roy, P. J. Hay, R. L. Martin, *J. Chem. Theory Comput.* **2008**, *4*, 1029.

[29] a) Y. Zhao, D. G. Truhlar, *J. Chem. Phys.* **2006**, *125*, 194101; b) Y. Zhao, D. G. Truhlar, *Theor. Chem. Acc.* **2008**, *120*, 215.

[30] W. Kuelche, M. Dolg, H. Stoll, H. Preuss, *Mol. Phys.* **1991**, *74*, 1245.

[31] a) C. Gonzalez, H. B. Schlegel, *J. Chem. Phys.* **1989**, *90*, 2154; b) C. Gonzalez, H. B. Schlegel, *J. Phys. Chem.* **1990**, *94*, 5523.

Received: November 13, 2012
Published online: January 31, 2013

